PNAS RESEARCH ARTICLE | MICROBIOLOGY

BRD9 functions as an HIV-1 latency regulatory factor

Tsz-Yat Luk[a,b], Lok-Yan Yim[a,b], Runhong Zhou[a,b], Yufei Mo[a,b], Huarong Huang[a,b], Meiqing Zhao[a,b], Jie Dai[a,b,c], Thomas Tsz-Kan Lau[a,b], Xiner Huang[b,d], Grace Chung-Yan Lui[e], Kwok-Yung Yuen[b,d,f,g], Jasper Fuk-Woo Chan[b,d,f,g], Alfred Sze-Lok Cheng[h], Zhiwei Chen[a,b,d,f,g,1], and Hin Chu[b,d,f,g,i,1]

Affiliations are included on p. 11.

Edited by John Coffin, Tufts University, Boston, MA; received September 11, 2024; accepted April 15, 2025

A major challenge for HIV type 1 (HIV-1) cure is the presence of viral latent reservoirs. The "Shock & Kill" strategy involves the combined use of latency reversal agents (LRA) and antiretroviral treatment (ART) to reactivate HIV-1 latent reservoirs, followed by elimination of infected cells. However, current LRAs are insufficient in fully reactivating the latent reservoirs. Therefore, investigation on novel HIV-1 latency regulators will be crucial to the success of HIV-1 cure research. Here, we identify bromodomain-containing protein 9 (BRD9) as an HIV-1 latency regulator. BRD9 inhibition induces HIV-1 latency reactivation in T cell lines, human resting memory CD4$^+$ T cells, and PBMCs derived from people living with HIV-1 (PWH) on ART. BRD9 inhibition, gene depletion, and protein degradation consistently reactivate HIV-1 latency. Moreover, BRD9 inhibition synergizes with BRD4 inhibition in inducing HIV-1 production. Mechanistically, BRD9 binds to HIV-1 LTR promoter and competes with HIV-1 Tat protein for binding to the HIV-1 genome. Additionally, our integrated CUT&RUN DNA sequencing, transcriptomics, and pharmacological analysis revealed downstream host targets of BRD9, including ATAD2 and MTHFD2, that modulate HIV-1 latency.

HIV-1 latency | AIDS | BRD9

AIDS remains a largely incurable disease despite decades of research. The primary cause of AIDS is the HIV, with HIV type 1 (HIV-1) being the most prevalent and transmissible variant globally due to its high variability (1). The main obstacle for achieving a complete cure for HIV-1 infection lies in the persistence of HIV-1 latency reservoirs within the resting memory CD4$^+$ T cell population of the host (2). This infected cell population is difficult to be eliminated because of its low gene replication rate, long lifespan, and clonal expansion capability (3). The latently infected cells maintain a low level of viral production, enabling them to evade recognition and immune response from cytotoxic T lymphocytes, macrophages, and other immunoregulatory factors (4).

The "Shock & Kill" strategy is an HIV treatment approach that combines LRA with ART (5). LRA reactivates HIV-1-infected latent cells and stimulates viral production, while ART interferes with HIV-1 viral replication (5). Currently, there are six major classes of well-established LRAs, including histone deacetylase (HDAC) inhibitors (6), histone methyltransferase (HMT) inhibitors (7), bromodomain and extraterminal domain (BET) protein inhibitors (8), protein kinase C (PKC) agonists (9), toll-like receptor (TLR) agonists (10), and immune checkpoint inhibitors (11). These LRAs target different epigenetic and cellular pathways to induce HIV-1 latency reactivation. However, current LRA treatments are unable to fully reactivate the HIV-1 latency reservoir, and replication-competent infected cells remain detectable in PWH on ART in clinical trials (12, 13), suggesting that crucial latency regulators remain to be identified. Therefore, exploring host targets that regulate HIV-1 latency and elucidating their downstream cellular pathways are critical for the development of future LRA regimens to achieve a more thorough reactivation of HIV-1 latency reservoir.

Here, we identified bromodomain-containing protein 9 (BRD9) as an HIV-1 latency regulator. We demonstrated that BRD9 inhibition significantly induced HIV-1 latency reactivation. Mechanistically, we revealed that BRD9 facilitates HIV-1 latency establishment through direct interaction with the HIV-1 genome and competition against the HIV-1 Tat protein. Furthermore, with integrated CUT&RUN DNA sequencing and transcriptomics, we revealed downstream cellular targets of BRD9, including ATAD2 and MTHFD2, which modulate HIV-1 latency. Together, our findings enhance our understanding on the regulatory mechanisms of HIV-1 latency and contribute to the development of future HIV-1 cure strategies.

Significance

HIV-1 infection remains incurable because of the long-lasting HIV-1-infected latency cells residing in the host. Current treatment strategies are unable to completely eliminate the virus latent reservoirs. Here, we identified bromodomain-containing protein 9 (BRD9) as an HIV-1 latency regulator. We found that BRD9 binds to both HIV-1 and host gene regulatory components that collectively modulate HIV-1 latency. BRD9 inhibition induces HIV-1 reactivation in multiple settings including peripheral blood mononuclear cells (PBMCs) from people living with HIV (PWH) on antiretroviral treatment (ART) and demonstrates synergistic effects with BRD4 inhibition. These findings enhance our understanding on the regulatory mechanisms of HIV-1 latency, which contributes to the development of future latency reversal agents (LRA) regimens for HIV-1 cure.

Author contributions: T.-Y.L., Z.C., and H.C. designed research; T.-Y.L., L.-Y.Y., R.Z., Y.M., H.H., M.Z., J.D., T.T.-K.L., and X.H. performed research; G.C.-Y.L., K.-Y.Y., J.F.-W.C., A.S.-L.C., Z.C., and H.C. contributed new reagents/analytic tools; T.-Y.L., Z.C., and H.C. analyzed data; and T.-Y.L., Z.C., and H.C. wrote the paper.

The authors declare no competing interest.

This article is a PNAS Direct Submission.

[1]To whom correspondence may be addressed. Email: zchenai@hku.hk or hinchu@hku.hk.

This article contains supporting information online at https://www.pnas.org/lookup/suppl/doi:10.1073/pnas.2418467122/-/DCSupplemental.

Published May 22, 2025.

Results

BRD9 Inhibitor Reactivates HIV-1 Latency in an Epigenetic Compound Screen. To identify targets that regulate HIV-1 latency and reactivation, we screened 280 candidates from an epigenetic compound library for their capacity in HIV-1 latency reactivation in ACH2 T cells by Enzyme-Linked Immunosorbent Assay (ELISA) (Fig. 1*A*). To identify candidates that regulate HIV-1 latency, we excluded compounds with well-established targets, including HDAC inhibitors, BRD4 inhibitors, HMT inhibitors, PKC agonists, TLR agonists, and immune checkpoint inhibitors. Our results prioritized I-BRD9 as an HIV-1 latency reversal agent, which increased HIV-1 viral production over the control by 10-fold (Fig. 1*B*). I-BRD9 is a specific inhibitor against BRD9, which functions as a transcription factor by recruiting other proteins, including GLTSCR1, BRG1, and SS18, to form the noncanonical BRG-/BRM-associated factor (ncBAF) complex and binds to genes for expression regulation (14). While BRD9 has been well characterized as a therapeutic target in cancer treatment (15), the role of BRD9 in HIV-1 latency was not known and was selected for subsequent investigations.

BRD9 Inhibition Reactivates HIV-1 Latency in ACH2 and J-Lat T Cells. To validate HIV-1 latency reactivation induced by BRD9 inhibition, we evaluated the impact of BRD9 inhibitor treatment on ACH2 and J-Lat T cells, which are HIV-1-infected latent T cell models. JQ-1 and dimethyl sulfoxide (DMSO) treatments were included as positive and negative controls, respectively. JQ-1 is a well-established HIV-1 LRA that targets BRD4 (16). To optimize the drug concentration for treatment, we treated ACH2 T cells with different concentrations of I-BRD9 and JQ-1 and selected the optimal concentrations based on cell viability and HIV-1 latency reactivation efficacy (*SI Appendix*, Fig. S1 *A* and *B*). Our results demonstrated that I-BRD9 significantly stimulated both HIV-1 LTR transcription initiation and Gag gene expression in a dose-dependent manner. Specifically, 10 μM I-BRD9 upregulated HIV-1 LTR transcription initiation by 2.3-fold ($P < 0.0001$) and HIV-1 Gag gene expression by 816-fold ($P < 0.0001$) when compared to DMSO (Fig. 1*C*). Similarly, by ELISA, we found that 5 μM and 10 μM I-BRD9 induced HIV-1 p24 production to 4.4-fold ($P = 0.0030$) and 16.1-fold ($P < 0.0001$) of DMSO, respectively (Fig. 1*D*). In flow cytometry assays, 10 μM I-BRD9 increased HIV-1 p24-positive cells from 2.5% in DMSO to 21.7% ($P < 0.0001$) (Fig. 1 *E* and *F*).

Next, we conducted I-BRD9 treatment on J-Lat T cells. We first selected treatment concentrations to be used in J-Lat T cells by examining and balancing HIV-1 viral production and cell viability (*SI Appendix*, Fig. S2 *A–E*). We found that I-BRD9 induced HIV-1 gene expression in J-Lat T cells in a dose-dependent manner. Treatment with 30 μM I-BRD9 stimulated HIV-1 LTR transcription initiation and HIV-1 Gag gene expression level by 116.2-fold ($P < 0.0001$) and 238.9-fold ($P < 0.0001$) when compared to DMSO, respectively (Fig. 1*G*). J-Lat T cells contain a GFP gene under the control of the HIV-1 LTR promoter (17). When HIV-1 gene transcription initiates, the GFP gene will express fluorescent signal. Therefore, we measured the intracellular fluorescent level of J-Lat T cells to validate HIV-1 gene transcription. We found that 30 μM I-BRD9 treatment increased the fluorescence level from 1.2% under DMSO treatment to an average of 10.8% ($P < 0.0001$) (Fig. 1*H*). These findings demonstrate that BRD9 inhibition significantly stimulates HIV-1 latency reversal in both ACH2 and J-Lat T cells.

BRD9 Depletion Reactivates HIV-1 Latency in ACH2 and J-Lat T Cells. We next seek to confirm target specificity by investigating the impact of BRD9 depletion in inducing HIV-1 latency reversal. We first employed BRD9 siRNA (siBRD9) to target the BRD9 gene while BRD4 siRNA (siBRD4) was included as a positive control. According to the qPCR results, siBRD9 reduced BRD9 gene expression in ACH2 T cells to 71.1% ($P < 0.0001$) of the scramble siRNA control (Fig. 2*A*). Following siBRD9 treatment, HIV-1 Gag gene expression and p24 protein production were increased to 141.3% ($P = 0.0210$) and 139.8% ($P = 0.0033$) of the scramble siRNA control, respectively (Fig. 2 *B* and *C*). Similarly, siBRD9 treatment significantly increased the intracellular HIV-1 p24 expression in ACH2 T cells (Fig. 2*D* and *SI Appendix*, Fig. S3*A*). Since the siRNA knockdown only partially reduced BRD9 gene expression, we next performed CRISPR/Cas9-based gene knockout for a more complete depletion of BRD9 protein in the J-Lat T cells (Fig. 2*E*). We showed that BRD9 knockout in J-Lat T cells induced HIV-1 LTR transcription initiation and Gag gene expression to 8.1-fold ($P = 0.0002$) and 8.9-fold ($P < 0.0001$) of the scramble sgRNA-treated cells, respectively (Fig. 2*F*). These results indicate that selective BRD9 gene depletion significantly stimulates HIV-1 latency reactivation.

In addition to genetic modification, we alternatively adopted a chemical approach to induce BRD9 protein degradation. VZ185, a selective BRD9 protein degrader was utilized for this purpose (18). We first confirmed that VZ185 robustly degraded BRD9 protein in ACH2 T cells (Fig. 2*G* and *SI Appendix*, Fig. S1*C*). Subsequently, we treated ACH2 T cells with increasing concentrations of VZ185 and assessed the impact of BRD9 depletion on HIV-1 latency reactivation. Our results revealed that VZ185 induced HIV-1 viral production and gene expression in a dose-dependent manner (Fig. 2 *H* and *I*). Specifically, 10 μM VZ185 increased HIV-1 LTR transcription initiation and HIV-1 Gag gene expression by 67.3-fold ($P < 0.0001$) and 169.2-fold ($P < 0.0001$) when compared to DMSO, respectively (Fig. 2*I*). Similarly, VZ185 induced intracellular HIV-1 p24 expression in a dose-dependent manner (Fig. 2*J*). Next, to verify VZ185 specificity, we treated BRD9 or control knockout J-Lat T cells with VZ185 and evaluated the level of HIV-1 Gag gene induction. Our results demonstrated that while VZ185 significantly induced HIV-1 Gag gene expression in the control (scramble sgRNA) knockout cells, VZ185 only modestly induced HIV-1 Gag gene expression in the BRD9 (BRD9 sgRNA) knockout cells beyond the HIV-1 Gag gene expression level already induced by BRD9 knockout (Fig. 2*K*). We included JQ-1 treatment on BRD4 knockout J-Lat T cells as a control, which similarly demonstrated reduced induction of HIV-1 Gag gene expression by JQ-1 upon BRD4 knockout (Fig. 2*K*). Interestingly, we observed a modest and comparable level of HIV-1 Gag gene induction by VZ185 and JQ-1 in BRD9 and BRD4 knockout J-Lat T cells, respectively. This is presumably due to the residue level of BRD9 and BRD4 protein still present in the mixed cell population after selection. Additionally, we explored the outcome of combined treatment of VZ185 and I-BRD9 on HIV-1 latency reactivation. The rationale is that if VZ185 specifically depletes BRD9 while I-BRD9 specifically inhibits BRD9, the two should have redundant functions on HIV-1 latency reactivation. Our results demonstrated that VZ185 induced HIV-1 viral production, intracellular p24 expression, and gene expression in a dose-dependent manner (*SI Appendix*, Fig. S3 *B–E*). Similarly, I-BRD9 treatment in the absence of VZ185 (VZ185 0 μM) elicited a similar trend in HIV-1 latency reversal (*SI Appendix*, Fig. S3 *B–E*). Nevertheless, when I-BRD9 was added in the presence of VZ185, it did not further induce HIV-1 latency reactivation beyond the impact of VZ185 (*SI Appendix*, Fig. S3 *B–E*). Together, these results confirmed the specificity of BRD9 manipulation in HIV-1 latency reversal.

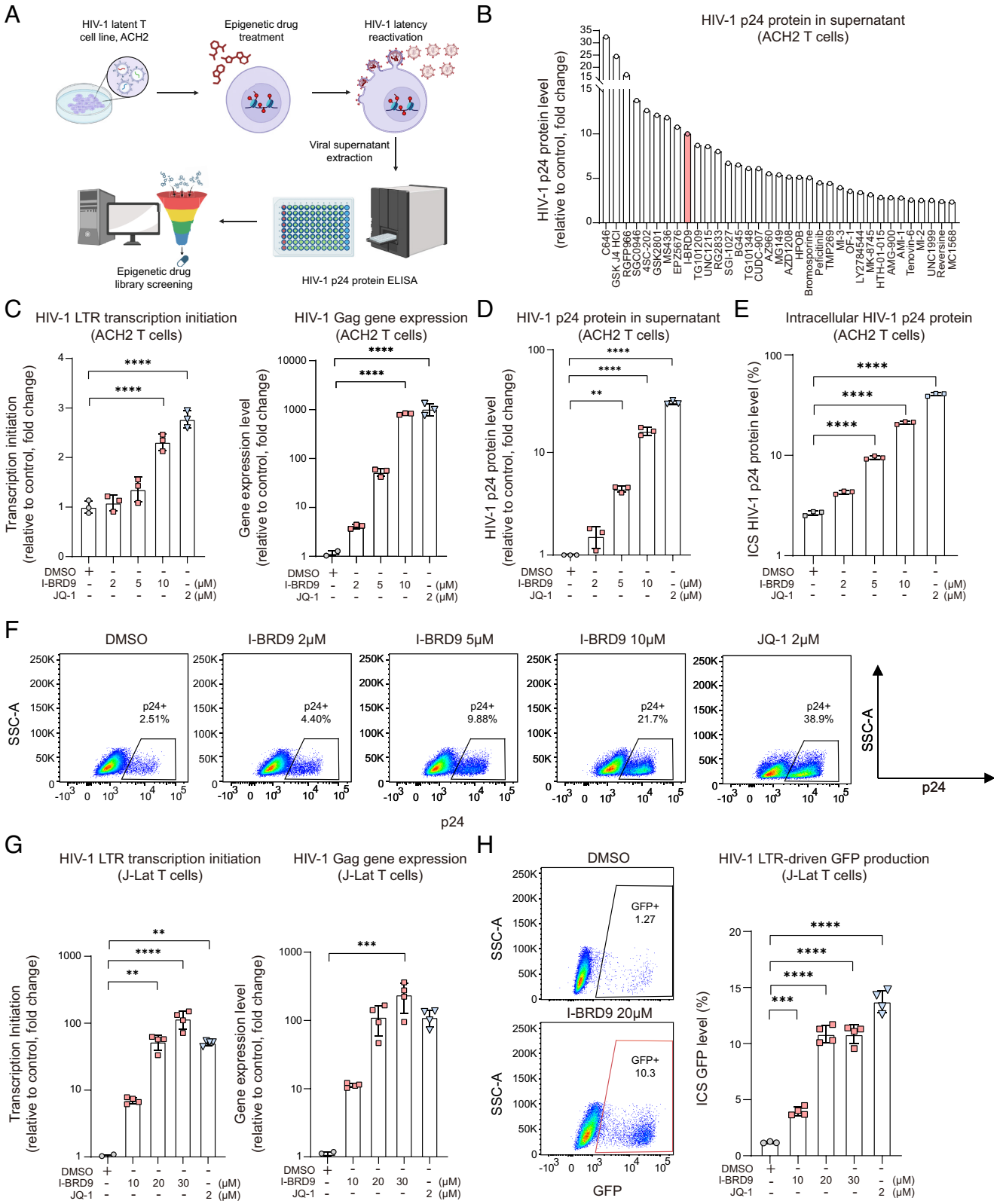

Fig. 1. BRD9 inhibition induces HIV-1 latency reactivation. (*A*) Schematic diagram of the epigenetic compound library screen. (*B*) Ranked list of epigenetic drug candidates in ACH2 T cells. HIV-1 latency reactivation was quantified with HIV-1 p24 ELISA (n = 3). (*C–F*) ACH2 T cells were treated with I-BRD9 or JQ-1. HIV-1 latency reactivation was quantified with qPCR (*C*), HIV-1 p24 ELISA (*D*), and flow cytometry (*E* and *F*) (n = 3). (*G* and *H*) J-Lat T cells were treated with I-BRD9 or JQ-1. HIV-1 latency reactivation was quantified with qPCR (n = 4) and flow cytometry (n = 3 for DMSO; n = 4 for I-BRD9 and JQ-1). Data represent mean ± SD. Statistical significance in (*C–E*, *G*, and *H*) was determined with one-way ANOVA with Dunnett multiple comparisons test. $^{**}P < 0.01$, $^{***}P < 0.001$, and $^{****}P < 0.0001$.

BRD9 Inhibition Synergizes with BRD4 Inhibition in HIV-1 Latency Reactivation. As different LRAs target distinct pathways in reactivating HIV-1 latency, combined LRA treatments may result in a more pronounced reactivation state. To this end, we investigated the potential synergistic effect of combining BRD9 inhibitor with other LRAs on HIV-1 latency reactivation. Our results demonstrated that 10 μM VZ185 induced an 18.3-fold (P = 0.0018) increase in HIV-1 viral protein production

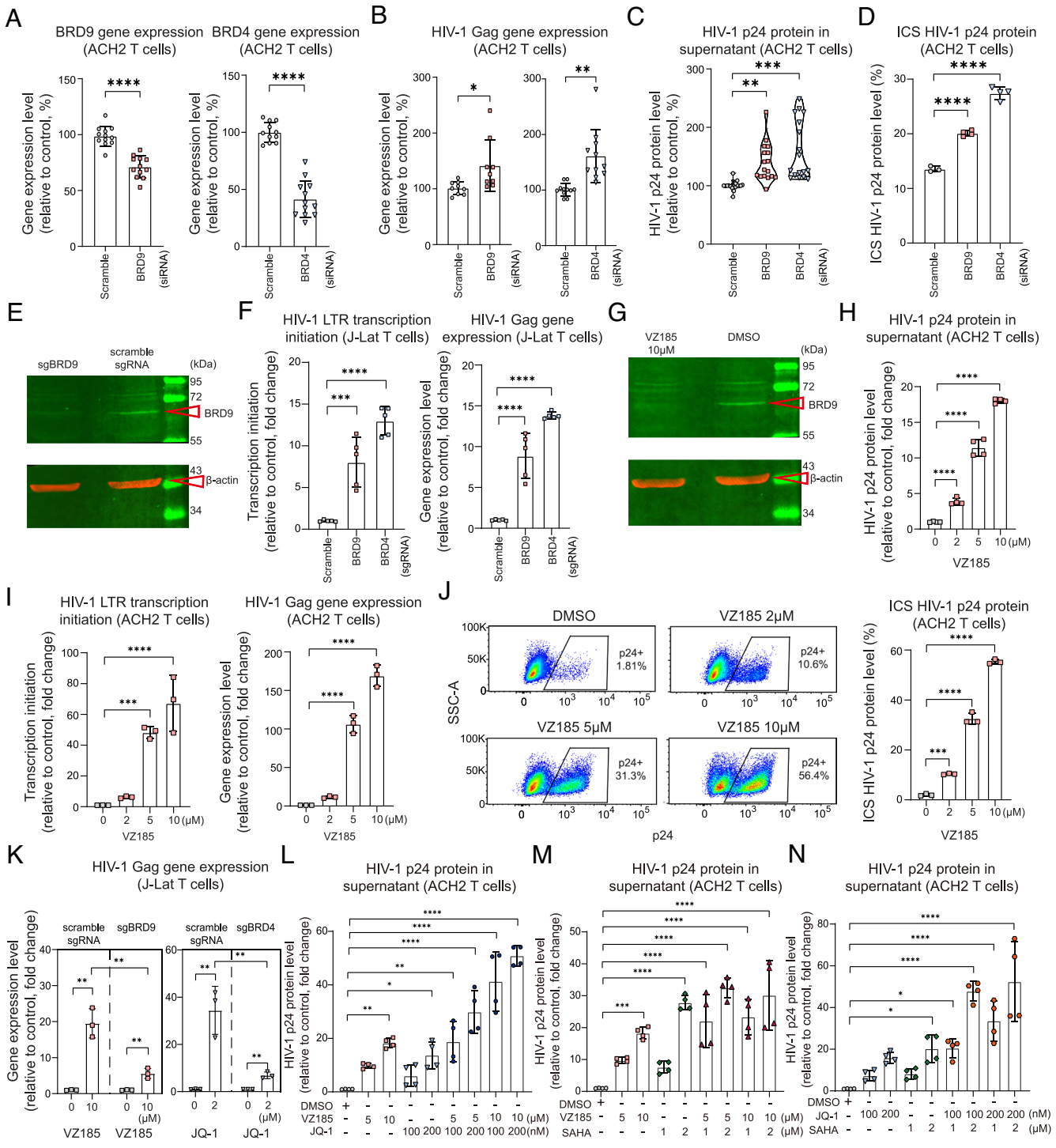

Fig. 2. Identification of BRD9 as an HIV-1 latency regulatory factor. (*A*) ACH2 T cells were treated with BRD9 or BRD4 siRNA. Knockdown efficiency was measured with qPCR (n = 12). (*B–D*) HIV-1 latency reactivation was quantified with qPCR (*B*) (n = 9 for the BRD9 panel, n = 11 for the BRD4 panel), ELISA (*C*) (n = 17), and flow cytometry (*D*) (n = 3 for scramble siRNA; n = 4 for BRD9 and BRD4 siRNA). (*E*) Representative Western blot image of BRD9 in BRD9 knockout J-Lat T cells. (*F*) HIV-1 gene expression in BRD9 or BRD4 knockout J-Lat T cells was quantified with qPCR (n = 5). (*G*) Representative Western blot image of BRD9 in VZ185-treated ACH2 T cells. (*H–J*) ACH2 T cells were treated with different concentrations of VZ185. HIV-1 expression was quantified with ELISA (n = 4) (*H*), qPCR (n = 3) (*I*), and flow cytometry (n = 3) (*J*). (*K*) BRD9 and BRD4 knockout J-Lat T cells were treated with VZ185 and JQ-1, respectively. HIV-1 Gag gene expression in the cell lysates was quantified with qPCR (n = 3). (*L*) ACH2 T cells were treated with VZ185 and JQ-1 in single or combined settings. HIV-1 latency reactivation was determined with ELISA (n = 4). (*M*) ACH2 T cells were treated with VZ185 and SAHA in single or combined settings. HIV-1 latency reactivation was determined with ELISA (n = 4). (*N*) ACH2 T cells were treated with JQ-1 and SAHA in single or combined settings. HIV-1 latency reactivation was determined with ELISA (n = 4). The same set of 5 μM VZ185 values was used in Fig. 2 *L* and *M* and *SI Appendix*, Fig. S4*A*; the same set of 10 μM VZ185 values was used in Fig. 2 *L* and *M*. Data represent mean ± SD. Statistical significance in (*A*, *B*, and *K*) was determined with the unpaired *t* test. Statistical significance in (*C*, *D*, *F*, *H–J*, and *L–N*) was determined with one-way ANOVA with Dunnett multiple comparisons test. **P* < 0.05, ***P* < 0.01, ****P* < 0.001, and *****P* < 0.0001.

compared to DMSO. Similarly, 200 nM JQ-1 increased HIV-1 viral protein production by 13.7-fold ($P = 0.0285$) (Fig. 2*L*). Importantly, the combined treatment of 10 μM VZ185 and 200 nM JQ-1 induced a 50.9-fold ($P < 0.0001$) increase in HIV-1 viral protein production (Fig. 2*L*), suggesting a synergistic effect in enhancing HIV-1 latency reactivation by simultaneous BRD9 and BRD4 inhibition. Interestingly, we did not observe an apparent synergistic effect between VZ185 and SAHA (Fig. 2*M* and

SI Appendix, Fig. S1*D*) but detected potential synergistic effects between JQ-1 and SAHA (Fig. 2*N*).

Next, we performed combined treatments on ACH2 T cells with a wider range of VZ185 and JQ-1 concentrations and conducted the zero-interaction potency (ZIP) analysis to evaluate synergy between VZ185 and JQ-1. We found that the ZIP synergy score for the combined treatment of VZ185 and JQ-1 in stimulating HIV-1 p24 production was 10.4, indicating the presence of the synergistic effect (*SI Appendix*, Fig. S4*A*). Similarly, the ZIP synergy scores for the combined treatment of VZ185 and JQ-1 in stimulating HIV-1 LTR transcription initiation and Gag gene expression were 35.3 and 145.0, respectively (*SI Appendix*, Fig. S4 *B* and *C*). Together, these results reveal a strong synergistic effect for the combined inhibition of BRD9 and BRD4 on HIV-1 latency reactivation in ACH2 T cells.

BRD9 Inhibitor Reactivates HIV-1 Latency in Infected Human Resting Memory CD4$^+$ T Cells and PBMCs from PWH under ART. To verify the potential of BRD9 inhibitor in reversing HIV-1 latency in human primary T cells, we performed HIV-1 infection on human resting memory CD4$^+$ T cells (CD4$^+$, CD45Ro$^+$, HLA-DR$^-$, CD25$^-$, CD69$^-$), which remained in a latent state after infection due to their resting nature (19). Afterward, we treated the cells with BRD9 inhibitor for 3 d to assess its impact on reactivating HIV-1 latency (Fig. 3*A*). We found that treatment with 10 μM and 20 μM I-BRD9 increased HIV-1 p24 production by 32.1% ($P = 0.0148$) and 47.3% ($P = 0.0002$) when compared to DMSO, respectively (Fig. 3*B*). Similarly, we observed a significant increase in intracellular HIV-1 p24 production following treatment with 20 μM I-BRD9, which increased the intracellular HIV-1 p24 level by 2.2-fold ($P = 0.0006$) when compared to DMSO (Fig. 3 *C* and *D*). In parallel, we performed cell surface staining for CD69, CD25, and HLA-DR and confirmed that none of the evaluated LRA induced T cell activation (*SI Appendix*, Fig. S5).

Next, we evaluated whether BRD9 inhibition could reactivate HIV-1 latency in PBMCs from PWH on ART. The PBMCs were first treated with I-BRD9 for 3 d to induce HIV-1 latency reversal. We then incubated the supernatant from I-BRD9-treated PBMCs with TZM-bl cells to perform the TZM-bl-cell-based quantitative viral outgrowth assay (TZM-bl qVOA) (Fig. 3*E*). Our results showed that 20 μM I-BRD9 induced a 48.1% ($P = 0.0037$) increase in HIV-1 viral production when compared to DMSO (Fig. 3*F*). Additionally, 20 μM I-BRD9 significantly increased the intracellular HIV-1 p24 level to 20.8% ($P < 0.0001$) from 4.3% under DMSO treatment (Fig. 3*G*). T cell activation was not induced by I-BRD9, indicating that the increased HIV-1 production was not due to T cell activation in these cells (*SI Appendix*, Fig. S6). To further evaluate the effect of BRD9 inhibition on HIV-1 gene expression in PBMCs from PWH on ART, we treated these PBMCs with different concentrations of VZ185. Our results demonstrated that VZ185 significantly induced HIV-1 Gag gene expression in these PBMCs in a dose-dependent manner. At 10 μM, VZ185 increased HIV-1 Gag gene expression by 2.9-fold ($P < 0.0001$) when compared to DMSO (Fig. 3*H*). Additionally, we performed combined I-BRD9 and VZ185 treatment in PBMCs from PWH on ART. Our data showed that in the absence of VZ185 (0 μM VZ185), I-BRD9 treatment dose-dependently increased HIV-1 Gag gene expression (Fig. 3*I*). However, upon 5 μM or 10 μM VZ185 treatment that already induced HIV-1 Gag gene expression through BRD9 degradation (Fig. 3*H*), I-BRD9 treatment did not further promote HIV-1 Gag gene expression (Fig. 3*I*). These results indicate that I-BRD9 and VZ185 specifically target the same target, BRD9, to induce latency reversal in PBMCs from PWH on ART. Next, we evaluated synergy between BRD9 and BRD4 inhibition in PBMCs from PWH on ART. We found that 5 μM VZ185 increased HIV-1 Gag gene expression by 1.6-fold and 200 nM JQ-1 increased HIV-1 Gag gene expression by 1.2-fold when added separately (Fig. 3*J*). When they were added simultaneously to the PBMCs, Gag expression was increased by 5.2-fold, which was much higher than the sum of the two single treatments combined (Fig. 3*J*). The Bliss Independence Model suggested synergy between VZ185 and JQ-1 (*SI Appendix*, Fig. S7 *A–C*) (20). Overall, our results indicate that BRD9 inhibition induces latency reactivation in PBMCs from PWH on ART and can be applied together with other LRA to achieve a synergistic effect on HIV-1 latency reactivation.

BRD9 Binds to the HIV-1 Genome and Competes with HIV-1 Tat Protein. After confirming the role of BRD9 in modulating HIV-1 latency reversal, we sought to investigate the underlying mechanism. We first evaluated whether BRD9 could suppress HIV-1 gene expression by binding to the HIV-1 genome. To this end, we performed the chromatin immunoprecipitation followed by the qPCR (ChIP-qPCR) assay to determine the interaction between BRD9 and the HIV-1 genome. BRD4 was included as a positive control since it was previously reported to inhibit HIV-1 gene transcription at the LTR promoter region (21). Rabbit IgG was used as a negative control. We utilized primary HIV-1-infected human resting memory CD4$^+$ T cells for this experiment. After fixation to stabilize the protein–chromatin complex, we lysed the cells and employed sonication to shear the chromatin. The DNA fragment size was between 300 base pair (bp) and 800 bp, indicating an appropriate fragment size range for this assay (Fig. 4*A*). Next, we performed pulldown assays using anti-BRD9 and anti-BRD4 antibodies to capture the protein–chromatin complex. Our results revealed that anti-BRD9 pulldowns had 8.0% ($P = 0.0003$) of the pulldown DNA carrying the HIV-1 LTR promoter region, which was significantly higher than that of the IgG control (Fig. 4*B*). Furthermore, the anti-BRD9 pulldown had 4.9% ($P = 0.0104$) of the pulldown DNA carrying the HIV-1 Gag gene region, whereas both the anti-BRD4 pulldown and the IgG control exhibited low binding to this region (Fig. 4*B*). Next, we treated HIV-1-infected resting memory CD4$^+$ T cells with I-BRD9 before conducting ChIP-qPCR. Our results showed that after 20 μM I-BRD9 treatment, the DNA level carrying the HIV-1 LTR promoter region from the anti-BRD9 protein pulldown decreased from 12.6% to 3.4% ($P = 0.0107$) (Fig. 4*C*), while the DNA level carrying the HIV-1 Gag gene region from the anti-BRD9 pulldown decreased from 7.4 to 3.6% ($P = 0.0031$) (Fig. 4*C*). These findings suggest that the BRD9 protein binds to the HIV-1 genome at the LTR promoter and Gag gene region, which can be attenuated by BRD9 inhibition. Previous research showed that BRD4 competes with HIV-1 Tat protein for binding at the HIV-1 LTR promoter region (16). We, therefore, evaluated whether BRD9 could suppress HIV-1 gene expression through a similar mechanism. We hypothesize that BRD9 protein may interfere with HIV-1 Tat protein binding at the HIV-1 LTR promoter region. When BRD9 is removed, HIV-1 Tat protein can replace its position and initiate HIV-1 gene transcription (Fig. 4*D*). To test this hypothesis, we conducted a modified CUT&RUN assay to evaluate HIV-1 Tat binding to HIV-1 LTR promoter with or without the presence of BRD9 in ACH2 T cells. Our results showed that the addition of BRD9 reduced the binding between HIV-1 Tat and the HIV-1 LTR promoter by 56% ($P = 0.0002$) (Fig. 4*E*). These results indicate that BRD9 competes with HIV-1 Tat in binding to the HIV-1 genome.

Next, we conducted CUT&RUN followed by DNA sequencing (CUT&RUN-seq) (22) to identify the precise binding sites of BRD9 on the HIV-1 genome. We utilized primary HIV-1-infected human resting memory $CD4^+$ T cells as our cell model and employed an anti-BRD9 antibody to pull down the BRD9 protein and its associated chromatin. For comparison, we included anti-BRD4 antibody and rabbit IgG as positive and negative controls, respectively. Additionally, we used anti-H3K27me3 antibody as another control to ensure accurate DNA cleavage and extraction. We verified the size distribution of DNA fragments from all four experimental groups for subsequent sequencing (*SI Appendix*, Fig. S8 *A–D*). Our results revealed that both BRD9 and BRD4 proteins could bind to the HIV-1 LTR promoter region (Fig. 4*F*). The aligned-read peak spectrum of the anti-BRD9 pulldown treatment appeared broader and more pronounced than that of the anti-BRD4 control. Furthermore, we found that both proteins could bind to the HIV-1 Env gene region, which was validated with ChIP-qPCR (Fig. 4*F* and *SI Appendix*, Fig. S9). To gain insights into the host genes bound by BRD9, we assigned the log-odds binding score of each motif occurrence on the genome with the CUT&RUN Tools CENTIPEDE package (23). This generated a ranked list of likely direct binding sites of BRD9, with ROCK1P1 and DUX4 genes emerged as the top two genes (Fig. 4 *G* and *H*). Importantly, we identified distinct binding motifs for BRD9 and BRD4 proteins, indicating that their DNA binding targets differ significantly (Fig. 4*I*). Collectively, we reveal that BRD9 binds to both viral and host targets to modulate HIV-1 latency.

Identification of Differentially Expressed Genes after BRD9 Depletion. To gain further insights into the downstream pathways modulated by BRD9, we treated ACH2 T cells with VZ185 for 2 d and collected samples for RNA transcriptome sequencing. (*SI Appendix*, Fig. S10 *A* and *B*). We ranked the genes based on their fold changes in expression level and *P*-values to generate heatmap and volcano plots (*SI Appendix*, Fig. S10 *C* and *D*). Additionally, we performed the Kyoto Encyclopedia of Genes and Genomes pathway analysis, which highlighted enriched pathways including cell–cell adhesion and regulation of the phosphorus metabolic process (*SI Appendix*, Fig. S10*E*). In the Gene Ontology analysis, the most significant pathways were found to relate to mitotic cell division and DNA replication (*SI Appendix*, Fig. S10*F*). For example, the chromosome segregation pathway was significantly enriched and we performed Gene Set Enrichment Analysis to illustrate the enrichment. The leading-edge gene subset showed close clustering, suggesting a significant difference in expression of this gene set in ACH2 T cells upon BRD9 depletion (*SI Appendix*, Fig. S10*G*). Additionally, we performed the Gene Set Variation Analysis to estimate the variation of the gene set enrichment among the samples. The highlighted gene sets that were upregulated in ACH2 T cells under VZ185 treatment including the JAK/STAT pathway, p53 signaling pathway, and cytokine-to-cytokine receptor interaction (*SI Appendix*, Fig. S11).

Integrated CUN&RUN-seq and Transcriptomic Sequencing Analysis Identified BRD9 Downstream Targets That Modulate HIV-1 Latency. Next, we employed the Binding and Expression Target Analysis program to integrate data from CUN&RUN-seq and transcriptomic sequencing, which allowed us to identify and group the BRD9-bound genes into upregulated and downregulated groups. We ranked these genes based on their binding intensity and correlation with BRD9 protein. The downregulated BRD9-bound genes following BRD9 depletion represent targets that may play a role in suppressing HIV-1 replication (Fig. 5*A*). As these BRD9-bound genes were downregulated during BRD9 inhibition, BRD9 likely serves as the expression activator of these downstream genes. They potentially have similar HIV-1 suppressive functions as that of BRD9 or have collaborative effects with BRD9 in HIV-1 latency modulation. Among the top-ranked genes from the list, we selected ATAD2, MTHFD2, LDHB, and BUB1B for subsequent analysis due to the presence of selective and well-defined inhibitor against these targets. We evaluated the effectiveness of AZ13824374 (ATAD2 inhibitor), DS18561882 (MTHFD2 inhibitor), AXKO-0046 (LDHB inhibitor), and BAY-1816032 (BUB1B inhibitor) single treatment and in combination with VZ185 to assess the presence of potential synergistic effects in inducing HIV-1 latency reactivation. We found that while AZ13824374 and VZ185 increased HIV-1 p24 production by 3.0-fold ($P = 0.044$) and 5.2-fold ($P = 0.0006$) when compared with DMSO, respectively (Fig. 5*B*), the combined treatment of AZ13824374 and VZ185 resulted in a 17.1-fold ($P < 0.0001$) increase in HIV-1 p24 production when compared with DMSO (Fig. 5*B*). Our qPCR results showed similar trends in stimulating HIV-1 LTR transcription initiation and Gag gene expression by AZ13824374 and VZ185 treatments (Fig. 5*C*). Thus, these results demonstrated that ATAD2 inhibition can significantly induce HIV-1 latency reversal and synergize with BRD9 inhibition to reactivate HIV-1 latency. Similar results were observed for DS18561882, AXKO-0046, and BAY-1816032 with all three drug candidates significantly stimulating HIV-1 latency reactivation and enhancing VZ185's latency reversal effect (Fig. 5 *B* and *C*). Next, we validated the function of the identified BRD9-regulated genes in PBMCs from PWH on ART. Our data demonstrated that AZ13824374, DS18561882, AXKO-0046, and BAY-1816032 all induced HIV-1 Gag gene expression in PBMCs from PWH on ART (Fig. 5*D*). Additionally, AZ13824374 and DS18561882 induced synergistic effect in HIV-1 latency reactivation together with VZ185, while AXKO-0046 and BAY-1816032 demonstrated a largely similar trend but did not reach statistical significance (Fig. 5*D* and *SI Appendix*, Fig. S12). Overall, these results confirmed the impact of our identified BRD9-regulated downstream genes on HIV-1 latency reactivation in PBMCs from PWH on ART.

Next, we further investigated the mechanism of the identified BRD9-regulated downstream genes on latency reversal. We focused our investigation on ATAD2 and MTHFD2 since their inhibitors demonstrated the best synergy with VZ185 in PBMCs from PWH on ART as shown in Fig. 5*D*. Through literature research, we found that both ATAD2 and MTHFD2 are potential transcription regulators that control gene expression (24–27). To this end, we evaluated the impact of AZ13824374 (ATAD2 inhibitor) and DS18561882 (MTHFD2 inhibitor) on the expression of a list of representative genes that are known to promote HIV-1 latency (*SI Appendix*, Fig. S13 *A* and *B*). Interestingly, we found that AZ13824374 and DS18561882 both inhibited the expression of CBX4, DEPDC5, FOXO1, FTSJ3, ORC1, PAF1C, PIWIL4, and ZNF304, suggesting that ATAD2 and MTHFD2 positively mediated the expression of these HIV-1 latency–promoting factors (*SI Appendix*, Fig. S13*A*). Together, our results suggest that BRD9 can promote HIV latency through ATAD2 and MTHFD2, which facilitate the expression of HIV-1 latency–promoting genes (*SI Appendix*, Fig. S14*A*). Inhibition of BRD9 results in reduced expression of ATAD2 and MTHFD2, which attenuate the expression of these HIV-1 latency–promoting genes, leading to HIV-1 latency reactivation (*SI Appendix*, Fig. S14*B*). Moreover, we investigated the upregulated BRD9-bound genes in ACH2 T cells under VZ185 treatment (Fig. 5*E*). These genes possessed increased expression upon BRD9 inhibition, indicating their positions as downstream factors suppressed by BRD9. We chose TXNIP and JAK3 as representative genes for downstream

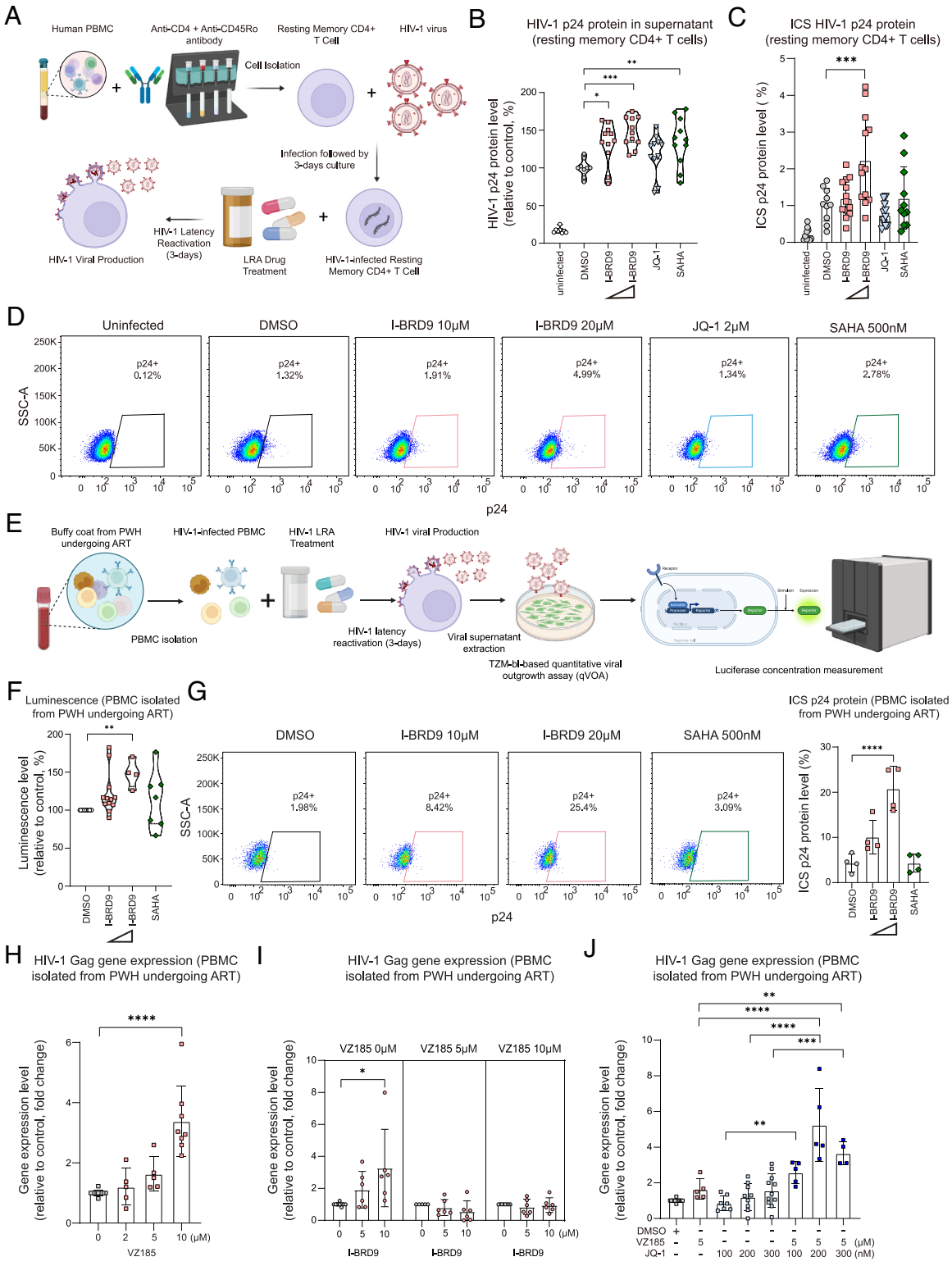

Fig. 3. BRD9 inhibition induces HIV-1 latency reactivation in HIV-1-infected human primary T cell models. (*A*) Schematic of the LRA treatment in human resting memory CD4$^+$ T cells. (*B* and *C*) HIV-1 infection was performed by spinoculation. The infected cells were treated with LRAs for 3 d. HIV-1 latency reactivation was determined with ELISA (n = 8 for uninfected; n = 9 for DMSO; n = 11 for I-BRD9, JQ-1, and SAHA) (*B*) or flow cytometry (n = 10 for uninfected and DMSO; n = 11 for JQ-1 and SAHA; n = 13 for I-BRD9) (*C*). (*D*) Representative flow cytometry dot plots. (*E*) Schematic of the LRA treatment in PBMCs from PWH on ART. (*F*) PBMCs from PWH on ART were treated with VZ185 or SAHA for 3 d. HIV-1 latency reactivation was quantified with TZM-bl qVOA (n = 13 for DMSO and 10 μM I-BRD9; n = 4 for 20 μM I-BRD9; n = 7 for SAHA). (*G*) PBMCs from PWH on ART were treated with VZ185 or SAHA for 3 d. HIV-1 latency reactivation was quantified with flow cytometry (n = 4). (*H*) PBMCs from PWH on ART were treated with different concentrations of VZ185 for 3 d. HIV-1 Gag gene expression was quantified with qPCR (n = 8 for DMSO and 10 μM VZ185; n = 5 for 2 μM and 5 μM VZ185). (*I*) PBMCs from PWH on ART were treated with VZ185 and different concentrations of I-BRD9 for 3 d. HIV-1 Gag gene expression was quantified with qPCR (n = 8 for DMSO and 10 μM VZ185; n = 5 for 5 μM VZ185; n = 6 for 5uM I-BRD9, 10 μM I-BRD9, and I-BRD9/VZ185 combined treatments). (*J*) PBMCs from PWH on ART were treated with VZ185 and JQ-1 in single or combined settings for 3 d. HIV-1 Gag gene expression was quantified with qPCR (n = 13 for DMSO; n = 7 for 100 nM JQ-1; n = 9 for 200 nM JQ-1; n = 11 for 300 nM JQ-1; n = 5 for 5 μM VZ185, 5 μM VZ185/100 nM JQ-1, and 5 μM VZ185/200 nM JQ-1 combined treatments; n = 4 for 5 μM VZ185/300 nM JQ-1 combined treatment). Data represent mean ± SD. Statistical significance in (*B*, *C*, and *F–J*) was determined with one-way ANOVA with Dunnett multiple comparisons test. **P* < 0.05, ***P* < 0.01, ****P* < 0.001, and *****P* < 0.0001.

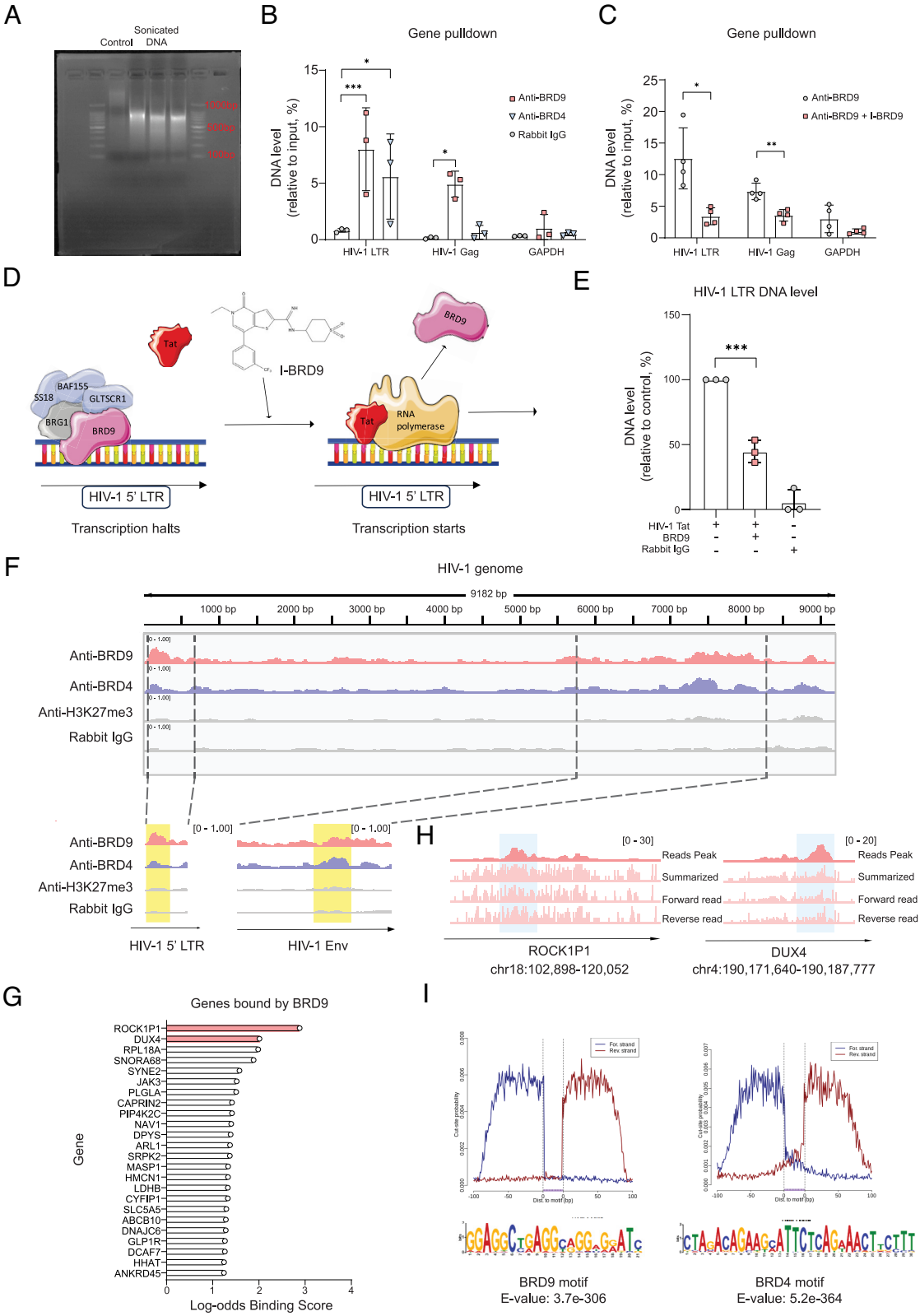

Fig. 4. Interaction of BRD9 with the HIV-1 genome and host genome of HIV-1-infected human resting memory CD4$^+$ T cells. (*A*) Representative DNA electrophoresis gel of sonicated DNA samples from HIV-1-infected human resting memory CD4$^+$ T cells. (*B*) ChIP-qPCR assay using anti-BRD9 and anti-BRD4 pulldown (n = 3). (*C*) ChIP-qPCR assay using anti-BRD9 pulldown under I-BRD9 treatment (n = 4). (*D*) Schematic of our working modeling on BRD9 binding to the HIV-1 genome. (*E*) Modified CUT&RUN assay that evaluates HIV-1 Tat protein binding to HIV-1 LTR promoter with or without added BRD9 protein in ACH2 T cells (n = 3). (*F*) CUT&RUN-seq reveals BRD9 and BRD4 binding region on the HIV-1 genome. (*G*) Ranked list of host genes bound by the BRD9 protein. (*H*) Aligned-read peak spectra of BRD9 protein on ROCK1P1 and DUX4. (*I*) Binding motif estimation of BRD9 and BRD4 protein on human T cell genome. Data represent mean ± SD. Statistical significance in (*B*, *C*, and *E*) was determined with one-way ANOVA with Dunnett multiple comparisons test. *P < 0.05, **P < 0.01, and ***P < 0.001.

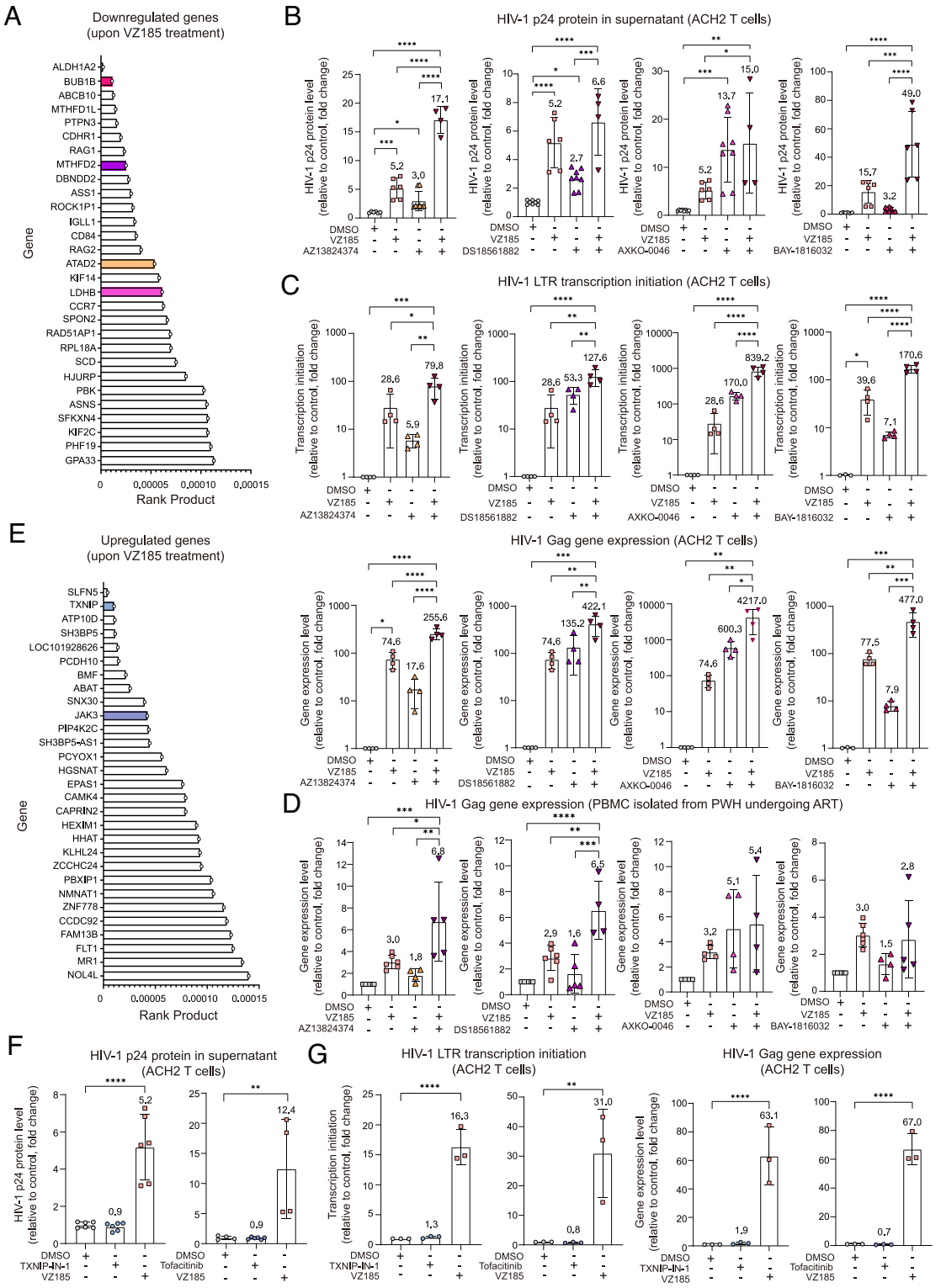

Fig. 5. Functional characterization of downstream cellular pathways of BRD9 in modulating HIV-1 latency. (*A*) Ranked list of downregulated BRD9-bound genes upon VZ185 treatment. (*B*) ACH2 T cells were treated with 10 μM VZ185, 10 μM AZ13824374, 10 μM DS18561882, 10 μM AXKO-0046, or 10 μM BAY-1816032 in single or combined settings. HIV-1 latency reactivation was quantified with ELISA (n = 6 for DMSO and VZ185; n = 8 for AZ13824374, DS18561882, AXKO-0046, and BAY-1816032; n = 4 for VZ185/AZ13824374, VZ185/DS18561882, VZ185/AXKO-0046 combined treatments; n = 6 for VZ185/BAY-1816032 combined treatment) (the same set of 10 μM VZ185 values was used in the AZ13824374, DS18561882, AXKO-0046 panels). (*C*) ACH2 T cells were treated with 10 μM VZ185, 10 μM AZ13824374, 10 μM DS18561882, 10 μM AXKO-0046, or 10 μM BAY-1816032 in single or combined settings. HIV-1 latency reactivation was quantified with qPCR (n = 4) (the same set of 10 μM VZ185 values was used in the AZ13824374, DS18561882, AXKO-0046 panels). (*D*) PBMCs from PWH on ART were treated with 10 μM VZ185, 10 μM AZ13824374, 10 μM DS18561882, 10 μM AXKO-0046, or 10 μM BAY-1816032 in single or combined settings. HIV-1 latency reactivation was quantified with qPCR (n = 5 for DMSO and DS18561882; n = 6 for VZ185; n = 5 for VZ185 (AXKO-0046 panel); n = 4 for AZ13824374, AXKO-0046, and BAY-1816032; n = 5 for VZ185/AZ13824374 and VZ185/BAY-1816032 combined treatment; n = 4 for VZ185/DS18561882 and VZ185/AXKO-0046 combined treatment) (the same set of 10 μM VZ185 values was used in the AZ13824374 and BAY-1816032 panels). (*E*) Ranked list of upregulated BRD9-bound genes upon VZ185 treatment. (*F* and *G*) ACH2 T cells were treated with 10 μM VZ185, 10 μM TXNIP-IN-1, or 10 μM tofacitinib. HIV-1 latency reactivation was quantified with ELISA (n = 6 for DMSO, VZ185, and TXNIP-IN-1; n = 4 for tofacitinib) (*F*) or qPCR (n = 3) (*G*). Data represent mean ± SD. Statistical significance in (*B*–*D*, *F*, and *G*) was determined with one-way ANOVA with post hoc Tukey's multiple comparisons test. **P* < 0.05, ***P* < 0.01, ****P* < 0.001, and *****P* < 0.0001.

analysis and found that neither TXNIP-IN-1 (TXNIP inhibitor) nor tofacitinib (JAK3 inhibitor) stimulated HIV-1 p24 production and gene expression (Fig. 5 *F* and *G*).

Discussion

Here, we identified BRD9 as an HIV-1 latency regulator. BRD9 functions as a transcription factor and forms the ncBAF complex with other proteins, including GLTSCR1, SMARCA2/4, SS18, and SMARCC2 (28). BRD9's bromodomain facilitates its recognition of the N-acetylated lysine on proteins such as histone for interaction with chromatin, while its DUF3512 domain functions to recruit and assemble other components of the ncBAF complex (28). A previous study reported that BRD9 and the ncBAF complex play a role in maintaining the antiviral state induced by interferon in cells (29). BRD9 also plays a role in maintaining chromatin accessibility, thereby regulating the cell fate of hematopoietic stem cells (14). These findings underscore the significance of BRD9 in epigenetic regulation of gene expression and highlight its potential as a therapeutic target.

We demonstrated that BRD9 inhibition stimulated HIV-1 latency reactivation in various human T cell models. Importantly, we observed a synergistic effect between BRD9 and BRD4 inhibition in stimulating HIV-1 latency reactivation in both T cell lines and PBMCs from PWH on ART. This finding signifies that BRD9 and BRD4 inhibition undergo distinct downstream pathways in reactivating HIV-1 latency and their effects are complementary. The potential of BRD9 inhibitor in enhancing the effects of other LRAs during combination treatments is particularly important since current LRA treatments are unable to completely reactivate the HIV-1 latency reservoir and replication-competent infected cells remain detectable in PWH on ART in clinical trials (12, 13), which suggest that unknown latency regulators remain to be identified. The identification of BRD9 in part fills in this important research gap and will contribute to the development of successful LRA regimens.

With ChIP-qPCR and CUT&RUN-seq, we revealed that BRD9 could bind to the HIV-1 LTR promoter region. Mechanistically, we demonstrated that BRD9 interfered with the binding of HIV-1 Tat to the LTR promoter region. This finding establishes BRD9 as another member of the BET family with the ability to modulate HIV-1 latency. Additionally, our CUT&RUN-seq and RNA sequencing combined analysis identified genes that were directly bound by BRD9 while were differentially expressed upon BRD9 depletion, including ATAD2 and MTHFD2. Through literature research, we found that ATAD2 and MTHFD2 are potential transcription regulators. ATAD2 is a well-defined epigenetic modulator that directly binds to chromatin, leading to increased chromatin accessibility, and regulates the gene expression of a specific set of genes (24). MTHFD2 is a one-carbon metabolism enzyme that can localize to the cell nucleus to maintain DNA and histone methylation (26). Recently, MTHFD2 was shown to modulate histone methylation and played an epigenetic modulatory role in T cells (27). These prior works hinted that ATAD2 and MTHFD2 may regulate gene expression that associate with HIV-1 latency. To this end, we found that inhibition of both ATAD2 and MTHFD2 attenuated the expression of a list of representative HIV-1 latency–promoting genes. Importantly, in addition to ATAD2 and MTHFD2 that we experimentally validated, we have revealed a repertoire of genes that may positively or negatively regulate HIV-1 latency. Most of these genes were not previously known to associate with HIV-1 latency. Therefore, they should be further explored as novel HIV-1 latency regulatory factors, and future investigations will be required to reveal the mechanisms behind these genes.

Our study has a number of limitations. First, we have not been able to conduct in vivo experiments to validate the HIV-1 latency modulation functions of the gene targets due to the difficulty of establishing a stable animal model carrying the long-lasting HIV-1 latency reservoir. Second, BRD9 may be capable of modulating HIV-1 latency through additional targets beyond the ones that were characterized in this study, which will require future investigations. As we have revealed in Fig. 5 *A* and *E*, BRD9 is a critical regulator of a repertoire of genes that may modulate HIV-1 latency. While it is not yet possible to perform in-depth investigation on the contribution of all identified genes toward HIV-1 latency in a single study, future investigations on the involvement of these genes in HIV-1 latency will advance our knowledge in this field.

In conclusion, our study reveals the HIV-1 latency modulatory function of BRD9 while identified BRD9 inhibitors as HIV-1 latency reversal agents. These findings will facilitate the identification of LRAs and the formulation of cocktail therapy, which will help target and eliminate the HIV-1 latency reservoir.

Materials and Methods

Virus and Cell Line, Human Resting Memory CD4$^+$ T Cells, and PBMCs from PWH on ART. ACH2 and J-Lat T cells were cultured in Roswell Park Memorial Institute (RPMI) 1640 medium with 10% fetal bovine serum (FBS), 1% penicillin–streptomycin, and 1% GlutaMAX. TZM-bl and MOLT4 cells were cultured in DMEM with 10% FBS, 1% penicillin–streptomycin, and 1% GlutaMAX. Buffy coats were donated by the Hong Kong Red Cross and PBMCs were isolated by Ficoll gradient separation as previously described (30, 31). Resting memory CD4$^+$ T cells were isolated from PBMCs by antibody staining and magnetic separation. Antibody kits used for cell isolation were the CD4$^+$ T cell isolation kit (EasySep), resting cell isolation kit (Miltenyi Biotec; CD25 MicroBeads II, CD69 MicroBead Kit II, Anti-HLA-DR MicroBeads, human) and memory T cell isolation kit (Miltenyi Biotec; CD45RO MicroBeads, human). Resting memory CD4$^+$ T cells were cultured in RPMI with 10% FBS, 1% penicillin–streptomycin, and 1% GlutaMAX. The studies involving PBMC from PWH on ART were approved by the Ethics Review Committee of the Joint Chinese University of Hong Kong-New Territories East Cluster Clinical Research Ethics Committee (2018.445). Written informed consent was received before participation. The use of human PBMCs was approved by the Institutional Review Board of the University of Hong Kong/Hospital Authority Hong Kong West Cluster (UW19-482, UW18-286, and UW19-833). Blood samples from PWH on ART were obtained by the Division of Infectious Diseases at the Department of Medicine and Therapeutics, the Chinese University of Hong Kong. The clinical characteristics of study participants are provided in *SI Appendix*, Table S1. PBMCs were cultured in RPMI with 10% FBS, 1% penicillin–streptomycin, and 1% GlutaMAX. HIV-1 JRFL was used in this study and was obtained from the NIH AIDS Research and Reference Reagent Program, USA.

Epigenetic Compound Library. The epigenetic compound library was purchased from Selleck Chemicals (Cat. No.: L1900).

Cell Viability Assay. We performed the MTT assay to measure the viability of cells after treatment. Cells were added onto 96-well plates with the respective drug treatment. After 2-d drug treatment, we applied MTT reagent for 3 h of incubation. Then, we added MTT solvent for 15 min and recorded the light absorbance of cell culture for cell viability measurement.

siRNA Gene Knockdown Assay. We used Accell Pharmacon siRNA for the gene knockdown experiment. We delivered the siRNA to cells with Accell siRNA delivery medium and incubated it with the cell culture for 4 d. We extracted cellular messenger ribonucleic acid (mRNA) to confirm the gene knockdown efficiency.

CRISPR/Cas9 sgRNA Gene Knockout. We used the lenti-CRISPR-V2 plasmid provided by IGE Biotechnology Company Limited for lentiviral construction. We transfected 293T cells with lenti-CRISPR-V2 plasmid, pMD2G plasmid, and psPAX2 plasmid for lentiviral construction for 2 d. After purification and

concentration of lentivirus, we performed lentiviral infection on ACH2 and J-Lat T cells together with polybrene supplementation. Then, puromycin was used to select for the lentiviral-transduced cells.

mRNA Extraction, RT-PCR, and qPCR Experiments. mRNA was extracted using the Qiagen RNA extraction kit. We reverse transcribed the mRNA samples into complementary DNA (cDNA) by RT-PCR and quantified the cDNA samples by qPCR. We normalized the expression levels of genes using GAPDH. The primer list is provided in *SI Appendix*, Table S2.

HIV-1 p24 ELISA. Supernatant from cell culture was collected and lysed with HIV-1 viral protein lysis buffer. Lysed samples were tested with the HIV-1 p24 ELISA kit (ZeptoMetrix).

Flow Cytometry Assay. Cell samples were washed and resuspended in Fluorescence-Activated Cell Sorting buffer containing 0.5% bovine serum albumin. The Zombie Aqua Fixable Viability Kit (BioLegend) was used to classify viable cells. Antibodies used for cell surface staining include PE anti-HLA-DR antibody (Abcam), PerCP/Cy5.5 anti-IL-2 Receptor alpha antibody (Abcam), APC anti-CD69 antibody (Abcam), Pacific Blue anti-human CD4 antibody (BioLegend) and PE/Cyanine7 anti-human CD45RO antibody (BioLegend). The BD Cytofix/Cytoperm Fixation/Permeabilization Kit was used to fix and permeabilize cells. The FITC-KC57 antibody (Coulter Clone) was used for HIV-1 p24 quantification in intracellular antibody staining.

TZM-bl qVOA. TZM-bl cells were seeded on 96-well plates. Viral supernatant was added to the cells and incubated for 2 d. The cells were then lysed and the luminescence signal was detected a luciferase assay system (Promega).

Protein Extraction and Western Blot Assay. Cell samples were lysed with Radioimmunoprecipitation assay buffer on ice. Samples were then boiled with protein loading buffer containing sodium dodecyl sulfate. Proteins were separated by gel electrophoresis and transferred onto polyvinylidene difluoride membrane. An anti-BRD9 antibody (Active Motif) and an anti-beta-actin antibody (Invitrogen) were used for detection.

ChIP-qPCR Assay. Cell samples were fixed with formaldehyde for crosslinking between protein and chromatin. Cell lysis was performed with sodium dodecyl-sulfate lysis buffer to release the enclosed protein–chromatin complex. Then, we performed sonication for six cycles of 10 s operation with 30 s intervals at 30% amplitude to shear the chromatin into short DNA fragments. Immunoprecipitation was performed at 4 °C overnight with an anti-BRD9 antibody (Active Motif), anti-BRD4 antibody (Abcam), anti-HIV-1 Tat antibody (Abcam), or rabbit IgG (Invitrogen). Reverse crosslinking between target protein and chromatin was performed with proteinase K digestion at 55 °C for 2 h. DNA purification was performed with the QIAamp DNA mini kit (Qiagen). qPCR was performed to identify the pulled down genes.

CUT&RUN-seq. CUT&RUN-seq was performed with the CUT&RUN Pro Complete Set (Antibodies-online). After immobilization of cell samples on Concanavalin A beads (Antibodies-online), permeabilization of cells was performed with digitonin-containing buffer. After that, antibody was added to samples and the mixture was incubated at 4 °C overnight. Then, the CUTANA pA/G-MNase enzyme (Antibodies-online) was added and incubated with samples at 37 °C for 1 h to cut the DNA bound by the target protein from the chromatin. After removing the bound protein and enzyme by proteinase K digestion at 50 °C for 1 h, we extracted and purified the DNA with the QIAamp DNA mini kit (Qiagen) for sequencing experiment. Library preparation and Illumina sequencing were conducted by Centre for PanorOmics Science (CPOS) at HKU. Pair-end DNA sequencing with 150 bp for each end was performed. CUT&RUNTools was utilized for the data analysis (22).

Modified CUT&RUN Followed by qPCR Experiment Demonstrating Chromatin-Binding Competition between BRD9 and HIV-1 Tat Protein. After immobilization of cell samples on concanavalin beads, permeabilization of cells was performed by digitonin-containing buffer. Recombinant human BRD9 protein (Abcam) and recombinant HIV-1 Tat protein (Abcam) were added to initiate protein–chromatin binding for overnight at 4 °C. Next, anti-HIV-1 Tat antibody (Invitrogen) was added to cells for overnight at 4 °C. Then, the CUTANA pA/G-MNase enzyme (Antibodies-online) was added. After removing the bound protein and enzyme with proteinase K digestion, we extracted and purified the DNA with the QIAamp DNA mini kit (Qiagen) for qPCR that quantified the protein–chromatin binding intensity.

RNA Sequencing. ACH2 T cells were treated with 10 μM VZ185 for 2 d and cell samples were collected for mRNA extraction and purification by the RNeasy Mini Kit (Qiagen). Library preparation and RNA sequencing were conducted by CPOS, HKU. Pair-end RNA sequencing with read length of 150 bp on each end was performed. The RNA sequencing data underwent quality control by FastQC, followed by reads filtering, reads alignment, and mapping onto human reference genome using the Bowtie2 program. Quantitative comparison of gene expression profiles between samples was processed by the DeSeq2 program. The R platform was utilized to perform calculation and construct figures.

Statistical Analysis. Statistical analysis was performed with GraphPad Prism. Unpaired *t* tests were used to evaluate the difference between two groups. When handling more than two groups of samples, we utilized one-way ANOVA. A *P*-value below 0.05 was considered statistically significant.

Figure Preparation. The figures were prepared using GraphPad Prism, Adobe Illustrator, and BioRender.

Data, Materials, and Software Availability. All study data are included in the article and/or *SI Appendix*.

ACKNOWLEDGMENTS. We acknowledge US NIH for providing the cell line and the virus. We also appreciate the Centre for PanorOmics Science (CPOS), HKU, for conducting the DNA and RNA sequencing experiment and the respective library construction. H.C. thanks Dr. Gallant Ho for his support on the Gallant Ho Outstanding Young Professorship. This work was supported by General Research Fund (17119122), Collaborative Research Fund (C7103-22G), and Theme-Based Research Scheme (T11-706/18-N), the Research Grants Council of the Hong Kong Special Administrative Region; Health@InnoHK, Innovation and Technology Commission, the Government of the Hong Kong Special Administrative Region.

Author affiliations: [a]AIDS Institute, School of Clinical Medicine, Li Ka Shing Faculty of Medicine, The University of Hong Kong, Hong Kong Special Administrative Region of China; [b]Department of Microbiology, School of Clinical Medicine, Li Ka Shing Faculty of Medicine, The University of Hong Kong, Hong Kong Special Administrative Region of China; [c]Institute for AIDS/STD Control and Prevention, Yunnan Centre for Disease Control and Prevention, Kunming, Yunnan 650500, China; [d]Center for Virology, Vaccinology and Therapeutics, Hong Kong Science and Technology Park, Hong Kong Special Administrative Region of China; [e]Division of Infectious Diseases, Department of Medicine and Therapeutics, The Chinese University of Hong Kong, Hong Kong Special Administrative Region of China; [f]State Key Laboratory of Emerging Infectious Diseases, The University of Hong Kong, Hong Kong Special Administrative Region of China; [g]Department of Clinical Microbiology and Infection Control, The University of Hong Kong-Shenzhen Hospital, Shenzhen, Guangdong 518053, People's Republic of China; [h]School of Biomedical Sciences, The Chinese University of Hong Kong, Hong Kong Special Administrative Region of China; and [i]Materials Innovation Institute for Life Sciences and Energy, The University of Hong Kong Shenzhen Institute of Research and Innovation, Shenzhen 518048, People's Republic of China

1. I. Sarabia, A. Bosque, HIV-1 latency and latency reversal: Does subtype matter? *Viruses* **11**, 1104 (2019).
2. N. M. Archin, J. M. Sung, C. Garrido, N. Soriano-Sarabia, D. M. Margolis, Eradicating HIV-1 infection: Seeking to clear a persistent pathogen. *Nat. Rev. Microbiol.* **12**, 750–764 (2014).
3. J. K. Wong *et al.*, Recovery of replication-competent HIV despite prolonged suppression of plasma viremia. *Science* **278**, 1291–1295 (1997).
4. L. B. Cohn, N. Chomont, S. G. Deeks, The biology of the HIV-1 latent reservoir and implications for cure strategies. *Cell Host Microbe* **27**, 519–530 (2020).
5. Y. Kim, J. L. Anderson, S. R. Lewin, Getting the "Kill" into "Shock and Kill": Strategies to eliminate latent HIV. *Cell Host Microbe* **23**, 14–26 (2018).
6. T. A. Rasmussen *et al.*, Panobinostat, a histone deacetylase inhibitor, for latent-virus reactivation in HIV-infected patients on suppressive antiretroviral therapy: A phase 1/2, single group, clinical trial. *Lancet HIV* **1**, e13–e21 (2014).
7. D. Boehm *et al.*, SMYD2-mediated histone methylation contributes to HIV-1 latency. *Cell Host Microbe* **21**, 569–579.e6 (2017).
8. Q. Niu *et al.*, Structure-guided drug design identifies a BRD4-selective small molecule that suppresses HIV. *J. Clin. Invest.* **129**, 3361–3373 (2019).
9. J. L. Sloane *et al.*, Prodrugs of PKC modulators show enhanced HIV latency reversal and an expanded therapeutic window. *Proc. Natl. Acad. Sci. U.S.A.* **117**, 10688–10698 (2020).

10. H. Z. Meas *et al.*, Sensing of HIV-1 by TLR8 activates human T cells and reverses latency. *Nat. Commun.* **11**, 147 (2020).
11. C. Gubser, C. Chiu, S. R. Lewin, T. A. Rasmussen, Immune checkpoint blockade in HIV. *EBioMedicine* **76**, 103840 (2022).
12. D. K. McMahon *et al.*, A phase 1/2 randomized, placebo-controlled trial of romidespin in persons with HIV-1 on suppressive antiretroviral therapy. *J. Infect. Dis.* **224**, 648–656 (2021).
13. H. M. Delagreverie, C. Delaugerre, S. R. Lewin, S. G. Deeks, J. Z. Li, Ongoing clinical trials of human immunodeficiency virus latency-reversing and immunomodulatory agents. *Open Forum Infect. Dis.* **3**, ofw189 (2016).
14. M. Xiao *et al.*, BRD9 determines the cell fate of hematopoietic stem cells by regulating chromatin state. *Nat. Commun.* **14**, 8372 (2023).
15. C. Zhang *et al.*, Aberrant activation of m6A demethylase FTO renders HIF2alpha(low/-) clear cell renal cell carcinoma sensitive to BRD9 inhibitors. *Sci. Transl. Med.* **13**, eabf6045 (2021).
16. Z. Li, J. Guo, Y. Wu, Q. Zhou, The BET bromodomain inhibitor JQ1 activates HIV latency through antagonizing Brd4 inhibition of Tat-transactivation. *Nucleic Acids Res.* **41**, 277–287 (2013).
17. G. Jiang *et al.*, Reactivation of HIV latency by a newly modified Ingenol derivative via protein kinase Cdelta-NF-kappaB signaling. *AIDS* **28**, 1555–1566 (2014).
18. V. Zoppi *et al.*, Iterative design and optimization of initially inactive proteolysis targeting chimeras (PROTACs) identify VZ185 as a potent, fast, and selective von Hippel-Lindau (VHL) based dual degrader probe of BRD9 and BRD7. *J. Med. Chem.* **62**, 699–726 (2019).
19. W. J. Swiggard *et al.*, Human immunodeficiency virus type 1 can establish latent infection in resting CD4+ T cells in the absence of activating stimuli. *J. Virol.* **79**, 14179–14188 (2005).
20. G. M. Laird *et al.*, Ex vivo analysis identifies effective HIV-1 latency-reversing drug combinations. *J. Clin. Invest.* **125**, 1901–1912 (2015).
21. E. Alamer, C. Zhong, R. Hajnik, L. Soong, H. Hu, Modulation of BRD4 in HIV epigenetic regulation: Implications for finding an HIV cure. *Retrovirology* **18**, 3 (2021).
22. Q. Zhu, N. Liu, S. H. Orkin, G. C. Yuan, CUT&RUNTools: A flexible pipeline for CUT&RUN processing and footprint analysis. *Genome Biol.* **20**, 192 (2019).
23. R. Pique-Regi *et al.*, Accurate inference of transcription factor binding from DNA sequence and chromatin accessibility data. *Genome Res.* **21**, 447–455 (2011).
24. A. Baggiolini *et al.*, Developmental chromatin programs determine oncogenic competence in melanoma. *Science* **373**, eabc1048 (2021).
25. Y. Morozumi *et al.*, Atad2 is a generalist facilitator of chromatin dynamics in embryonic stem cells. *J. Mol. Cell Biol.* **8**, 349–362 (2016).
26. N. Pardo-Lorente *et al.*, Nuclear localization of MTHFD2 is required for correct mitosis progression. *Nat. Commun.* **15**, 9529 (2024).
27. A. Sugiura *et al.*, MTHFD2 is a metabolic checkpoint controlling effector and regulatory T cell fate and function. *Immunity* **55**, 65–81.69 (2022).
28. X. Wang *et al.*, Author correction: BRD9 defines a SWI/SNF sub-complex and constitutes a specific vulnerability in malignant rhabdoid tumors. *Nat. Commun.* **10**, 4445 (2019).
29. J. Borold *et al.*, BRD9 is a druggable component of interferon-stimulated gene expression and antiviral activity. *EMBO Rep.* **22**, e52823 (2021).
30. H. Chu *et al.*, Tetherin/BST-2 is essential for the formation of the intracellular virus-containing compartment in HIV-infected macrophages. *Cell Host Microbe* **12**, 360–372 (2012).
31. H. Chu *et al.*, Middle east respiratory syndrome coronavirus efficiently infects human primary T lymphocytes and activates the extrinsic and intrinsic apoptosis pathways. *J. Infect. Dis.* **213**, 904–914 (2016).